Is F_1-ATPase a rotary motor with nearly 100% efficiency? Quantitative analysis of chemomechanical coupling and mechanical slip

Tomonari Sumi[1,2,*] **and Stefan Klumpp**[3,4]

[1]Research Institute for Interdisciplinary Science, Okayama University, 3-1-1 Tsushima-Naka, Kita-ku, Okayama 700-8530, Japan.
[2]Department of Chemistry, Faculty of Science, Okayama University, 3-1-1 Tsushima-Naka, Kita-ku, Okayama 700-8530, Japan.
[3]Institute for the Dynamics of Complex Systems, University of Göttingen, Friedrich-Hund-Platz 1, 37077 Göttingen, Germany.
[4]Department Theory and Bio-Systems, Max Planck Institute of Colloids and Interfaces, 14424 Potsdam, Germany.

ABSTRACT

We present a chemomechanical network model of the rotary molecular motor F_1-ATPase which quantitatively describes not only the rotary motor dynamics driven by ATP hydrolysis but also the ATP synthesis caused by forced reverse rotations. We observe a high reversibility of F_1-ATPase, i.e., the main cycle of ATP synthesis corresponds to the reversal of the main cycle in the hydrolysis-driven motor rotation. However, our quantitative analysis indicates that torque-induced mechanical slip without chemomechanical coupling occurs under high external torque and reduces the maximal efficiency of the free energy transduction to up to several ten percent below the optimal efficiency. Heat irreversibly dissipates not only through the viscous friction of the probe, but also directly from the motor due to torque-induced mechanical slip. Such irreversible heat dissipation is a crucial limitation for achieving a 100% free-energy transduction efficiency with biological nanomachines, since biomolecules are easily deformed by external torque.

KEYWORDS

F_1-ATPase, rotary molecular motor, chemomechanical network model, free-energy transduction efficiency, ATP synthesis, torque-induced mechanical slip

Many active processes in cells are based on the function of molecular motors, which convert chemical (free) energy into work [1,2]. These molecular motors provide realizations of nanometer-scaled thermodynamic machines and can thereby act as test cases for the recently developed stochastic thermodynamics that applies to such small isothermal systems [3-5]. The paradigmatic system of this type is a molecular motor working against an external load force or torque, while provided with a given concentration of its fuel (such as ATP) [6,7] or, more generally, of the reactants involved in the chemical process that powers the motor (such as ATP, ADP, and inorganic phosphate (Pi)) [8-10]. Key questions for understanding the thermodynamics of these motors are the efficiency and reversibility of that energy conversion. In this context, the rotary motor F_1-ATPase has played an important role due to its reversibility. F_1-ATPase is the catalytic domain of the F_oF_1-ATP synthase that in cells synthesizes ATP from ADP and Pi using a proton flux through the membrane-embedded F_o protein as the free-energy input [11-14]. In vitro, F_1 alone acts as a rotary motor, rotating the central γ subunit against the hexagonally arranged subunits $\alpha_3\beta_3$ [6,13,15-18], driven by the hydrolysis of ATP. Consistent with its function as an ATP synthase in vivo, it has been demonstrated that a forced reverse rotation of the γ subunit causes ATP synthesis [19,20]. By contrast, the linear motors kinesin-1 and myosin-V have been shown to hydrolyze ATP under forced backward motion due to superstall loads [21-23] or to move backwards with neither hydrolysis nor synthesis of ATP [24,25], respectively. Related to the issue of how a motor responds to superstall loads are the questions whether a stalled motor is in thermodynamic equilibrium [26] and what the maximal efficiency of the chemomechanical free-energy transduction is. Different definitions for the efficiency of molecular motors have been used [27]. Here we use the classical thermodynamic definition as the ratio of work done to chemical energy consumed by the system (or work done per forward step divided ATP hydrolysis energy times the average number of ATP molecules consumed during the forward step). For kinesin-1 the latter is estimated to be about 0.56 based on tight coupling of ATP hydrolysis and stepping with one molecule of ATP hydrolyze per step forward [28,29], but lower efficiencies have been determined by including ATP-dependent backward steps or chemical slip cycles [22,23]. These events reflect the irreversibility of the working cycle and irreversible internal heat dissipation [30-32] where more than one ATP molecules are, on average, consumed during a forward step under load [23,25]. For F_1-ATPase, however, the reversibility of the working cycle [19,20] and recent progress in understanding the energetics of the motor [9,10,33-36] suggest a tight coupling between the chemical reactions and the mechanical rotation and the possibility of nearly 100% chemomechanical free-energy transduction efficiency [9,10].

F_1-ATPase has been theoretically studied by molecular simulations [37-47] and stochastic modeling [27,48-54]. However, only a few quantitative studies have investigated the energetics of F_1-ATPase [27,52]. Here, we use a chemomechanical network approach to the F_1-ATPase to address those questions, based on the network theory originally introduced for linear motors such as kinesin-1 [55-58].

The network approach is based on the known reaction scheme for F_1-ATPase [6,18,33,59-63], while allowing for alternative working cycles, and describes the F_1 both in the rotary motor mode and in the ATP synthesis mode. We compare the theoretical results with data from recent experiments on the external-torque-dependent rotational rate against different viscous loads and under various chemical conditions and on the heat that irreversibly dissipates through the viscous friction of a probe [9,64]. The comparison indicates an important role for torque-induced mechanical slip, which limits the efficiency of chemomechanical free energy transduction. The motor's efficiency is rather high, but remains substantially below 100%. The energetics revealed by our analysis is interpreted by means of the trade-off relation between heat arising from the viscous friction of the probe and heat caused by the mechanical slip. In addition, our approach also sheds light on the kinetics of the motor as represented by a network structure consisting of multiple chemomechanical cycles. Pi release is the second rate-limiting process and plays a role as the trigger of the torque generation by the 40º rotation that is the primary rate-limiting step [62]. These results are consistent with atomistic molecular dynamics simulation as well [40,41,44-46].

Chemomechanical network modeling of F_1-ATPase. To describe the dynamics of the rotary molecular motor F_1-ATPase, we make use of a systematic chemomechanical network approach that was previously used for linear molecular motors [23,25,55,58]. This approach starts by identifying the chemical states of all motor subunits. F_1-ATPase is composed of the $\alpha_3\beta_3$ stator hexagonal ring and the rotary shift of the γ subunit, which is inserted into the $\alpha_3\beta_3$ ring [15]. The catalytic sites are located at the interfaces between the α and β subunits, mainly on each β subunit. Thus, three catalytic sites are arranged 120º apart around the γ subunit. Each catalytic site can be empty (E), occupied by ATP (T), by ADP and Pi (DP), and by ADP (D) or Pi (P), as assumed previously in several models [48,49,65-67]. Thus the $\alpha_3\beta_3$ ring can attain $4^3 = 64$ possible chemical states. To simplify this network and to reduce its size we merge the hydrolyzed ADP.Pi state into the ATP state and furthermore only consider the occupancy number of the catalytic sites shown in Fig. 1a. Thus, the nucleotide state in each catalytic site is not explicitly identified in this simplified model, while the chemical reaction that takes place in one of the three catalytic sites is expressed as the transition between those states: the vertical downward and upward edges correspond to ATP release and binding, respectively; the edges pointing toward the lower left and toward the upper right direction describe the release and binding of ADP, respectively; the edges pointing toward the lower right direction and toward the opposite direction are the release and binding of Pi, respectively. Each facet of this diagram corresponds to one conceivable chemical cycle of the motor. However, based on experimental observations, not all these cycles are used. Indeed, experiments point towards the subspaces A or B indicated by the red or blue transparent rhombus panel shown in Fig. 1a as the basic chemical cycles

in the chemomechanical network of F_1-ATPase.

It has been shown that the rotation of F_1-ATPase occurs in steps of 120º, each driven by hydrolysis of one ATP molecule [33,68], and the 120º step consists of 80º and 40º substeps [18,59,69,70]. The 80º substep is driven by ATP binding and the 40º substep by release of ADP or Pi [18]. Two models for the 120º step of F_1-ATPase that are consistent with these observations are shown in Fig. 1b and 1d, based on the subspaces of chemical states, A and B, respectively. The 0º dwell (after the 40º substep) waiting for ATP binding is considered as having the loose packing conformations of the $\alpha_3\beta_3$ ring, while the 80º dwell (after the 80º substep) waiting for ADP or Pi release is considered as having the tight packing conformations [40-42,44,46,71]. In Figs. 1b and 1d, the black horizontal arrows from state 1 (T^3) to state 5 ($<T^3>$) and from state 7 ($<T^2E>$) to state 3 (T^2E) indicate the forward 80º and 40º substeps, respectively. In addition, we introduce 120° forward and backward torque-induced mechanical slip transitions, indicated by the black cyclic arrows at the 80º and 40º dwells (see also Calculation details in the Supporting Information (SI)). Such mechanical slip can be caused by a distortion of the F_1-ATPase due to high external torque. The impact of the mechanical slip transitions is discussed below by comparing the experimental observations with the theoretical results for the models with and without mechanical slip. In Figs. 1b and 1d, the three circles with the letters T, D, P, and E and the black thick short arrow represent the chemical states of the catalytic sites on the three β subunits and the angular position of the γ subunit, respectively. The single and double asterisks added to the letter T indicate that the ATP molecule has already being bound during more than a one-step (120º) or than a two-steps (240º) rotation, respectively. As a result, the double asterisk implies the tightly closed conformation in the catalytic domain ready for the chemical reaction, Pi release or ADP release (e.g. the 5-to-8 or 5-to-6 transition, respectively, in Figs. 1b or 1d).

The models shown in Figs. 1b and 1d thus incorporate the reaction schemes and the chemical states that have been proposed based on experimental observations [60,61,63]. We note the one-to-one correspondence between the two models due to the identical network topology and chemical reactions, despite the fact that the chemical states assigned for each catalytic site are different in these two models. For instance, both the 8-to-7 transitions in Figs. 1b and 1d correspond to Pi release. In the following, we will use the notations of model A, but all our results apply to model B as well. Thus, our theoretical modeling cannot discriminate between these two models, but it can reveal which of the transition pathways, i.e. |587> or |567> appears in the main working cycle on the ATP-driven forward rotation. Thereby, this model allows us to test the proposed reaction scheme [44-46,61], that is, whether or not the torque generation upon the 40º substep is triggered by Pi release (the 8-to-7 transition). Details of the network modeling are provided in the SI text.
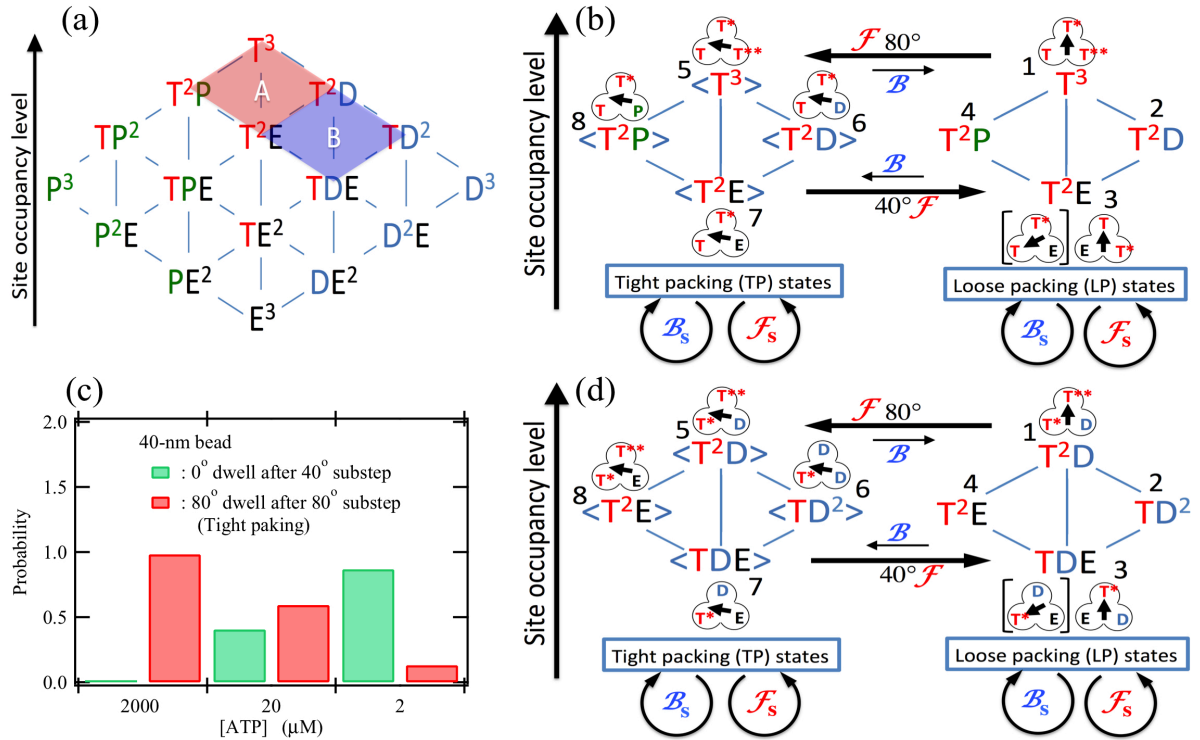
Figure 1. Chemomechanical network modeling of F$_1$-ATPase. (a) An occupancy diagram of three catalytic sites by the nucleotide molecules, ATP (T), ADP (D), and inorganic phosphate Pi (P). The edges correspond to chemical reactions and "E" denotes the empty for a catalytic site. (b) and (d) Chemomechanical network models of F$_1$-ATPase that are formed using respectively the state spaces A and B indicated by red and blue transparent rhombus panels in Fig. 1a. (c) The probabilities of the 0º dwell state (waiting for ATP binding) after 40º substep and of the 80º dwell state after 80º substep, at three ATP concentrations. These values are for the case observed with the use of a 40-nm bead [18] calculated by the eight-state model shown in Fig. 1b. In Figs. 1b and 1d, the black horizontal arrows indicate the rotational transitions with 80º or 40º that are coupled to the chemical transitions, while the black cyclic arrows indicate rotational slip transitions with 120º that are forced by external torque. The three circles with the letters T, D, P, and E and the black thick short arrow represent the chemical states of the catalytic sites on the three β subunits and the angular position of the γ subunit, respectively. The single and double asterisks added to the letter T indicate that the ATP molecule has already being bound during more than a one-step (120º) rotation and more than a two-steps (240º) rotation, respectively. The chemical states shown in these models basically accord to the reaction schemes proposed on the basis of experimental observations [60,61,63]. The four chemical states at the 0º dwell (after 40º substep) and at the 80º dwell (after 80º substep) are respectively supposed to have the loose packing and tight packing conformations, that have been demonstrated by molecular dynamics simulations [40,41,44,46].

Motor properties of F$_1$-ATPase. First of all, to validate the eight-state model shown in Fig. 1b, we compare motor properties of F$_1$-ATPase calculated with the eight-state model to the experimental data. Figure 1c shows the probabilities of the 0° dwell state after the 40° substep (waiting for ATP binding) and of the 80° dwell state after the 80° substep at ATP concentrations of 2 mM, 20 μM, and 2 μM. The results obtained by the eight-state model are consistent with the histograms of angular positions experimentally determined by the stepping rotation of a 40-nm bead [18]. At the lowest ATP concentration (2 μM), the probability of the 0° dwell is higher than that of the 80° dwell, indicating that ATP binding is a rate-limiting process. At the highest ATP concentration (2 mM), the probability of the 80° dwell is higher than that of the 0° dwell, implying that either ADP release, Pi release or the 40° substep is a rate-limiting process.

Figure 2a compares our theoretical results to experimental data [18] for the rotation rate V subject to two different loads attached the motor, a 40-nm bead and a 1-μm actin filament. In the model, the effect of viscous friction of the probe on the rotation rate is taken into considerate by multiplying the rates of all forward and backward mechanical transitions by a single scaling factor. The use of this single scaling factor leaves the steady-state balance condition intact [23,56,72] and does not affect the chemical transitions. For both probes, the rotation rates increase with increasing ATP concentration and saturates at different maximum values.

Next, we turn to the thermodynamic properties of the motor. Toyabe *et al.* performed experiments under different thermodynamic conditions, specifically constant chemical potential and a constant ATP concentration using a 287-nm bead as the probe [10]. Figures 2b and 2c show the torque dependence of the rotation rate V at various concentrations of ATP, ADP, and Pi. In Fig. 2b, a chemical potential difference $\Delta\mu$ is held constant through the conditions [ATP]=[ADP] and [Pi]=1 mM, while in Fig. 2c, [ADP] and [Pi] are varied to control $\Delta\mu$ under constant [ATP] = 10 μM. Here, $\Delta\mu$ is defined as the difference of the chemical potentials between one ATP molecule and one ADP plus one Pi molecule, i.e., $\Delta\mu = k_\mathrm{B}T\ln\{K_{eq}[\mathrm{ATP}]/[\mathrm{ADP}][\mathrm{Pi}]\}$ [73] with the equilibrium constant K_{eq}= 4.9 x 10^{11} μM [8]. In both conditions, the eight-state model with mechanical slip provides a good agreement with the experimental results [10]. The rotation rate V decreases as the external torque increases and a forced reverse (clockwise) rotation occurs at external torques larger than the stall torque τ_stall. Under the constant $\Delta\mu$ conditions [Fig. 2b], the values of τ_stall are very close to each other, even though the concentrations of ATP and ADP vary widely (subject to the constraint [ATP]=[ADP]). On the other hand, in Fig. 2c, the stall torque τ_stall obviously depends on the concentrations of ADP and Pi, even if the ATP concentration is constant. The relationship among $\Delta\mu$, τ_stall, and the effect of the mechanical slip will be discussed in Fig. 3.

In Fig. 2d, the ratio of the number of backward (clockwise) rotations to the number of forward (anticlockwise) rotations is shown in semi-logarithm scale as a function of external torque.

The results given by the eight-state models with and without the mechanical slip transitions agree well with the experimental data from ref. [10]. The effect of the mechanical slip is very small, indicating that this external torque dependence is attributable to the response of the chemomechanical coupling to the external torque.
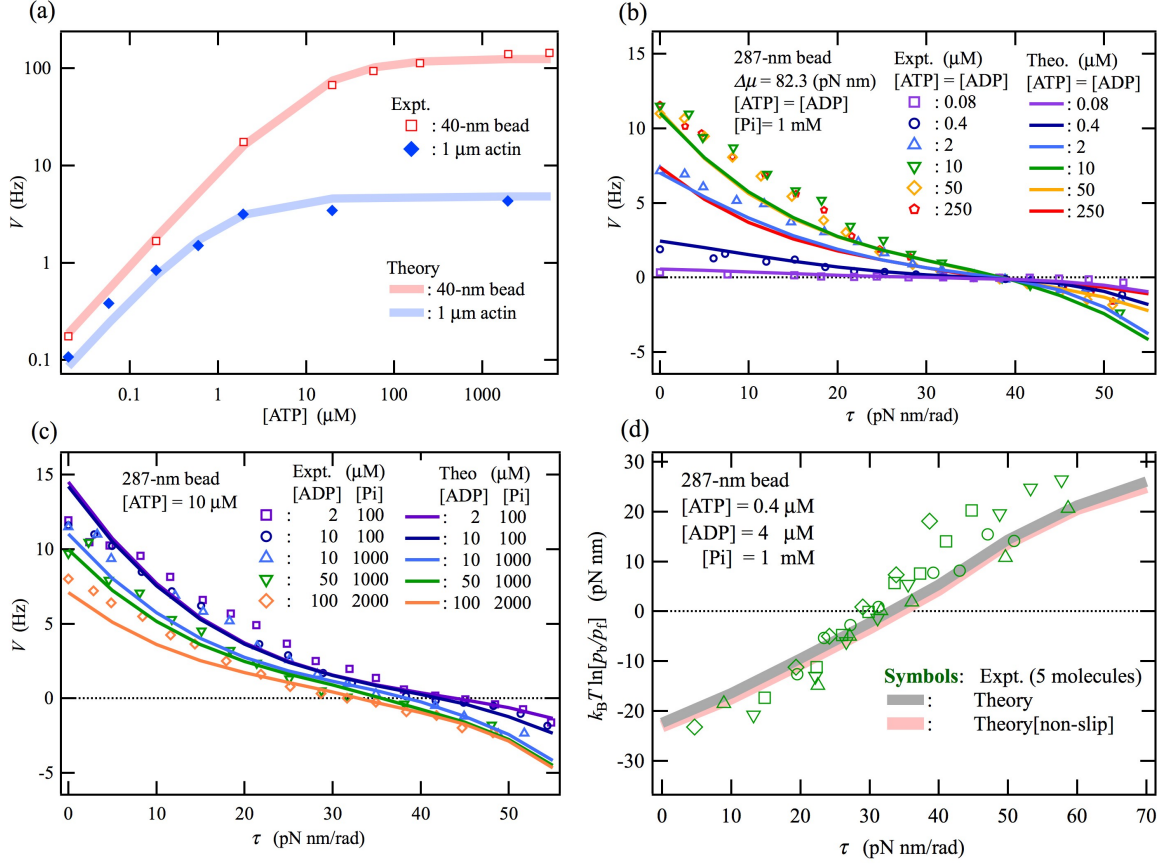
Figure 2. Motor properties of F_1-ATPase. (a) ATP-concentration dependences of the rotation rate V using a 40-nm bead and a 1-μm actin filament as the probe. (b) and (c) External torque dependences of the rotation rate V using a 289-nm bead as the probe at various concentrations of ATP, ADP, and Pi; (b) [ATP]=[ADP] and [Pi]=1 mM where the chemical potential difference $\Delta\mu$ is kept to be constant and (c) [ATP] = 10 μM while [ADP] and [Pi] are varying to control $\Delta\mu$. (d) The ratio of the number of backward (clockwise) rotations to the number of forward (anticlockwise) rotations as a function of external torque using the 289-nm bead as the probe at 0.4 μM ATP, 4 μM ADP, and 1 mM Pi. In Fig. 2d, the result obtained from the non-slip model, where no mechanical slip transitions are introduced into the eight-state model, is also shown for the comparison. The experimental results shown in (a) and (b)-(d) are provided by Yasuda *et al.* [18] and Toyabe *et al.,* [10] respectively.

Impact of the mechanical slip on the maximum work and efficiencies. Next, we compare the eight-state model with and without mechanical slip – hereafter we call the latter case the non-slip model – to examine effects of mechanical slip on motor properties. Figures 3a and 3b show the

maximum work done by the 120° rotation at the stall torque τ_{stall}, $W_{\text{stall}} = (2\pi/3)\tau_{\text{stall}}$, again under the two conditions of (a) constant $\Delta\mu$ and (b) constant ATP concentration as in Figs. 2b and 2c, respectively. In Fig. 3b, the experimental values for W_{stall} are plotted as a function of $\Delta\mu$ that is provided by the equilibrium constant K_{eq}= 4.9 x 10^{11} μM [8]. Note that our $\Delta\mu$ values for each condition differ slightly from the values given by Toyabe *et al.* [10] because we use a different value for K_{eq} than they did. The non-slip model gives values of W_{stall} that are almost equivalent to those obtained in the tight-coupling limit, i.e. $\Delta\mu$. Under constant chemical potential (Fig. 3a), the experimental values of W_{stall} [10] show clear deviations from the constant W_{stall} value in the tight-coupling limit (and thus also the non-slip model). These are particularly pronounced for low concentrations of ATP and ADP. Thus, the stall torque τ_{stall} depends on the concentrations of ATP and ADP, even when $\Delta\mu$ is kept constant [see also Fig. S2a in the SI text]. Likewise, the experimental W_{stall} values [10] deviate from the results of the non-slip model (Fig. 3b) and the discrepancy increases with increasing $\Delta\mu$. These results are consistent with experimentally observed torque-induced mechanical slip behavior whose importance has been argued in the biological function point of views [74].

By contrast, the results obtained from the eight-state model with mechanical slip agree well with the experimental data in both cases. These observations indicate that the tight-coupling limit, which yields the perfect efficiency of the free-energy transduction, is not achieved by F$_1$-ATPase and suggests that mechanical slip rotations that are caused by high external torques (stall or superstall torque) are the main reason for the observed reduction in that efficiency. Here, it should be noted that, in the case where the mechanical slip would occur, the stall torque is determined by the condition $V = V_{\text{chem}} + V_{\text{slip}} = 0$ where V_{chem} is the contribution to the rotation rate caused by the chemomechanical coupling, i.e., $V_{15} + V_{73}$, and V_{slip} is that caused by the mechanical slip, i.e., $V_L + V_T$ (see Calculation details in the SI text). The rotation rate provided by the non-slip model corresponds to the former V_{chem}. The large deviation of τ_{stall} from the tight-coupling limit at low concentrations of ATP and ADP [Fig. 3a] and the increase in the deviation from the tight-coupling limit with increasing $\Delta\mu$ [Fig. 3b] are quantitatively explained by the balance between V_{chem} and V_{slip}, as shown by Figs. S2b and S2d in the SI text. Similar deviations of W_{stall} from the non-slip model value are also observed under different constant $\Delta\mu$ conditions, see Fig. S3. The quantitative analysis indicates that, under the stall torque, F$_1$-ATPase is in a mechanical equilibrium, but not in thermodynamic equilibrium, where the ATP-driven forward rotation and the torque-induced mechanical (backward) slip occur with equal frequency, so that $V = V_{\text{chem}} + V_{\text{slip}}$ becomes zero.

Figure 3c shows the chemomechanical free-energy transduction efficiency, $\eta_{\text{m}} \equiv W /(\text{free energy gain}) = (2\pi V/3)\tau/(\Delta\mu\Delta J[\text{hydrolysis}])$, as a function of external torque τ again for a 287-nm bead as load [10] and under the constant $\Delta\mu$ condition of Fig. 3a. Here W is the work done by

8

the 120° rotation, and ΔJ[hydrolysis] is the total excess flux caused by ATP hydrolysis, $\Delta J_{56} + \Delta J_{87} + \Delta J_{12} + \Delta J_{43}$. It should be noted that the definition of η_{m} for an isothermal molecular motor is different from the usual definition of the efficiency of a heat engine such as a Carnot cycle, $\eta_{\mathrm{c}} = W/Q_H$ with the heat provided by a high-temperature heat bath Q_H. For a heat engine, the definition of η_{m} would rather correspond to $W/(Q_H - Q_L)$ with the heat absorbed by a low-temperature heat bath Q_L, thus, a Carnot cycle always has $\eta_{\mathrm{m}} = 1$. At low external torques (below 15 pN nm/rad for the nucleotide concentrations used here), the torque dependence of η_{m} agrees perfectly with that of the tight-coupling limit, $2\pi\tau/3\Delta\mu$. However, η_{m} turns to decrease with further increase of the external torque τ. The maximum of η_{m} is found between 0.4 and 0.8 in this condition and the external torques at which the maximal efficiencies are obtained are less than 85 % of the torque expected for perfect efficiency (39.4 pN nm). The obtained maximum value of η_{m}, 0.8, for $\Delta\mu = 20\, k_B T$ is consistent with an experimentally determined value 0.72 for $\Delta\mu = 31.25\, k_B T$ [75], since the higher $\Delta\mu$ is, the lower the maximum efficiency is, in a similar manner as the slight reduction of W_{stall} from $\Delta\mu$ (Fig. 2b and Fig. S3). The efficiency η_{m} of the non-slip model follows the tight-coupling limit up to τ_{stall}, where it suddenly drops down to zero due to small contributions of futile chemical slip cycles such as |1431>, |1231>, |7587>, and so on. In fact, the working cycle becomes very slow in the vicinity of stall torque τ_{stall}, thus these very slow futile chemical slip cycles occur during the long dwell times for rotation transitions.

9
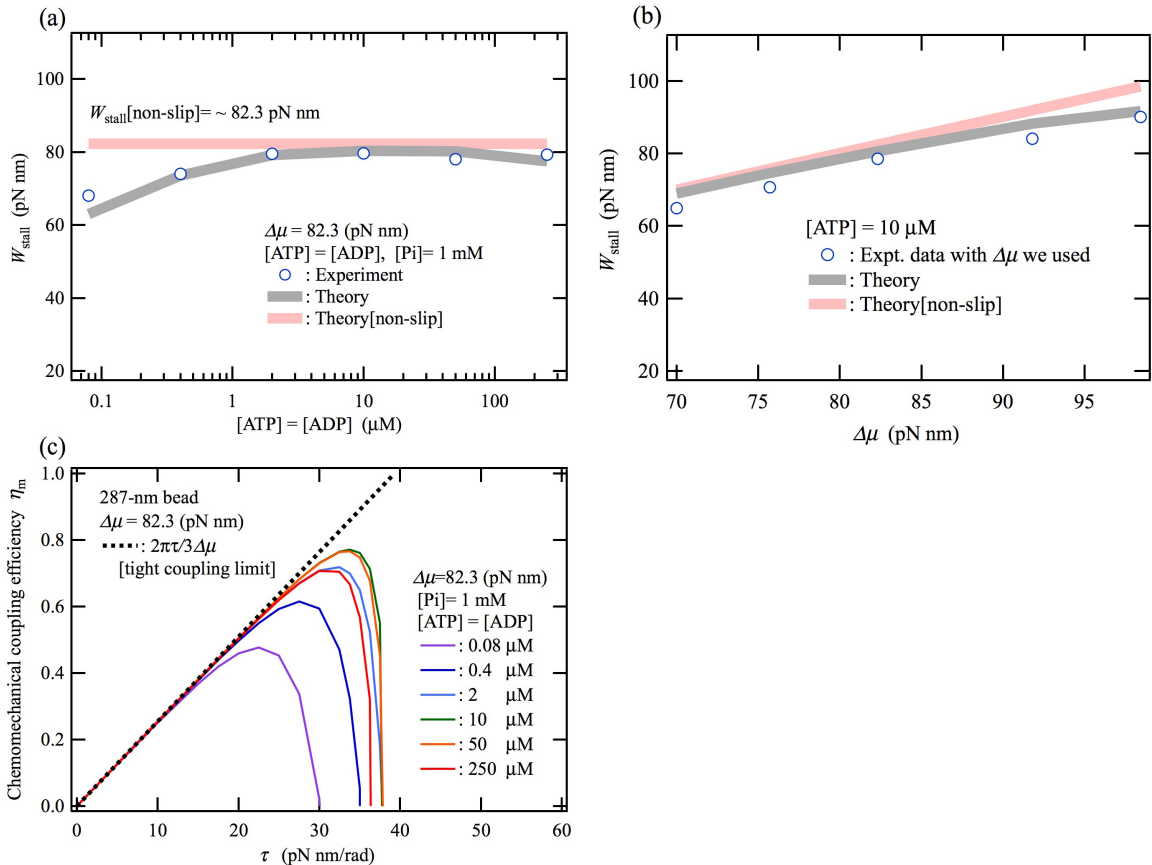
Figure 3. Maximum work done by the 120° rotation at the stall torque τ_{stall}, $W_{\text{stall}} = (2\pi/3)\tau_{\text{stall}}$. (a) ATP and ADP concentration dependence of W_{stall} under the condition [ATP]=[ADP] and [Pi]=1 mM (i.e. under the constant $\Delta\mu$ condition). (b) $\Delta\mu$ dependence of W_{stall} at varying [ADP] and [Pi] under fixing [ATP]= 10 μM. The conditions used in Figs. 3a and 3b are same as those in Figs. 2b and 2c, respectively. (c) Chemomechanical free-energy transduction efficiencies $\eta_{\text{m}} = (2\pi V/3)\tau/(\Delta\mu\Delta J[\text{hydrolysis}])$ of F$_1$-ATPase as a function of external torque τ with the use of a 287-nm bead under the constant $\Delta\mu$ condition as in (a), where V is the rotation rate and $\Delta J[\text{hydrolysis}]$ is the total excess flux caused by ATP hydrolysis. In (a) and (b), the results without the mechanical slip transitions, i.e., those by the non-slip model, are also shown as red thick lines. In Fig. 3b, the experimental values of W_{stall} are plotted as a function of $\Delta\mu$ that is determined using K_{eq}= 4.9 x 10^{11} μM ^{8} as the equilibrium constant. In (c), η_{m} in the tight-coupling limit is also shown as a black dashed line. The experimental results shown in (a) and (b) are based on the results provided by Toyabe *et al.* [10]

The energetics of ATP synthesis by F₁-ATPase. Finally, we examine the impact of mechanical slip on the energetics of the F$_1$ motor working in the synthase mode, i.e. synthesizing ATP while mechanically driven with a torque $\tau > \tau_{\text{stall}}$. Figure 4a shows the clockwise rotation rates as a function of the external torque in the synthase regime for the full eight-state model and the non-slip model in comparison with experimental data from ref. [64]. All experiments shown in Fig. 4 used a 300-nm bead ([ATP]=[ADP]=10 μM and [Pi]=1 mM, [64] thus $\Delta\mu$ was equal to 20.0$k_{\text{B}}T$). The clockwise rotation rate obtained from the eight-state model exceeds that of the non-slip model and gives better agreement with the experimental data than the non-slip model, especially at high external torque.

Figure 4b shows the heat that dissipates in the non-slip model during 120° rotation, $Q'[\text{non-slip}]$, and the experimentally determined heat that irreversibly dissipates during 120° rotation through the viscous friction of the probe, Q'_{probe}, [64] as a function of external torque. From the first law of thermodynamics, the heat that dissipates per unit time, Q, and heat generated per 120° rotation, Q', are given by the difference between the input of mechanical work by the external torque and the free-energy gain due to the ATP synthesis as follows:

$$Q = -2\pi\tau V - \Delta\mu\Delta J[\text{synthesis}], \tag{1a}$$

$$Q' = -[2\pi\tau V + \Delta\mu\Delta J[\text{synthesis}]]/(3|V|) \quad (V \neq 0), \tag{1b}$$

where V is negative in the synthesis regime and $\Delta J[\text{synthesis}]$, which is equivalent to $-\Delta J[\text{hydrolysis}]$, is positive. In the tight-coupling limit, all heat $Q'[\text{tight-coupling}]$ irreversibly dissipates through the viscous friction of the probe; thus, it is obtained as $(2\pi/3)\tau - \Delta\mu$ from Eq. (1b) using the tight-coupling condition $|\Delta J[\text{synthesis}]/V| = 3$. The heat that dissipates in the non-slip

model $Q'[\text{non-slip}]$ corresponds to the heat that dissipates through the viscous friction of the probe because the non-slip model is considered to be in nearly tight-coupling limit. However, $Q'[\text{non-slip}]$ seems to be slightly smaller than the experimentally determined Q'_{probe} [Fig. 4b]. This is because the rotation rate by the non-slip model is lower than the experimental value as shown in Fig. 4a.

Figure 4c shows the heat generated per unit time as obtained from the full eight-state model, Q, and from the non-slop model, $Q[\text{non-slip}]$, as a function of the external torque. For comparison, the experimental Q_{probe} value, which is determined by $Q_{\text{probe}} = 3|V| \times Q'_{\text{probe}}$, is also included (to calculate Q_{probe}, the theoretical value of the rotation rate V from the eight-state model was used which agreed well with the experimental values of V as seen in Fig. 4a). The comparison shows that the experimental heat, Q_{probe}, exceeds $Q[\text{non-slip}] = 3|V[\text{non-slip}]| \times Q'[\text{non-slip}]$ for larger external torques. This is because $|V|$ becomes larger than $|V[\text{non-slip}]|$ when the external torque is increased and furthermore the heat generated through the viscous friction of the probe Q'_{probe} is always larger than $Q'[\text{non-slip}]$, as shown in Fig. 4b, again due to $|V| > |V[\text{non-slip}]|$. On the other hand, the full eight-state model give values for the heat that slightly exceed the experimental values, even though the same rotation rate V is used to evaluate both. The difference can be interpreted as excess heat that is contained in Q but not Q_{probe} and that is irreversibly dissipated directly from the F_1 synthase, not through the viscous load. Figure 4d plots this excess heat, $Q_{\text{motor}} = Q - Q_{\text{probe}}$, as a function of external torque and shows that it increases with increasing torque.

In a recent study, Kawaguchi et al. presented a totally asymmetric allosteric model (TASAM) where a potential is switched during chemical transitions under spatially continuous fluctuations of the γ subunit rotation [52]. They applied it to the experimental data by Toyabe et al. [10] and concluded that the ATP-synthesis regime is exothermic whereas the ATP-hydrolysis motor regime turns to being endothermic at the stall torque as a boundary [52]. In the ATP synthesis regime, their result seems to be consistent with the result obtained here from the eight-state model, but in the ATP-hydrolysis regime the two models give opposite results. In addition, their model leads to the perfect free-transduction efficiency, $W_{\text{stall}} = \Delta\mu$, under the stall torque condition, $F_{\text{stall}} = 3\Delta\mu/2\pi$ (see the SI text), which is inconsistent with the experimental results by Toyabe et al. [10], as shown by Fig. 3. Furthermore, the absolute value of internal heat dissipation $|Q_{\text{motor}}/\Delta\mu|$ is significantly larger in their model than in ours and the $\Delta\mu$ dependence of $|Q_{\text{motor}}/\Delta\mu|$ is the opposite of ours (Fig. S4). Within our approach, the origin of the internal heat dissipation is different, as it results from mechanical slippage due to load torque, thus the internal heat dissipation is always exothermic and continuously varying by the load torque. On the other hand, the internal heat dissipation by their model is attributed to the irreversibility of the switching transitions, thus the switching transitions during the forward and backward rotation always causes endothermic and exothermic heat, respectively. Further support for our mechanical slip model is provided by the qualitative agreement

with the experimentally determined value of the mechanochemical coupling efficiency of ATP synthesis [Fig. S5a].
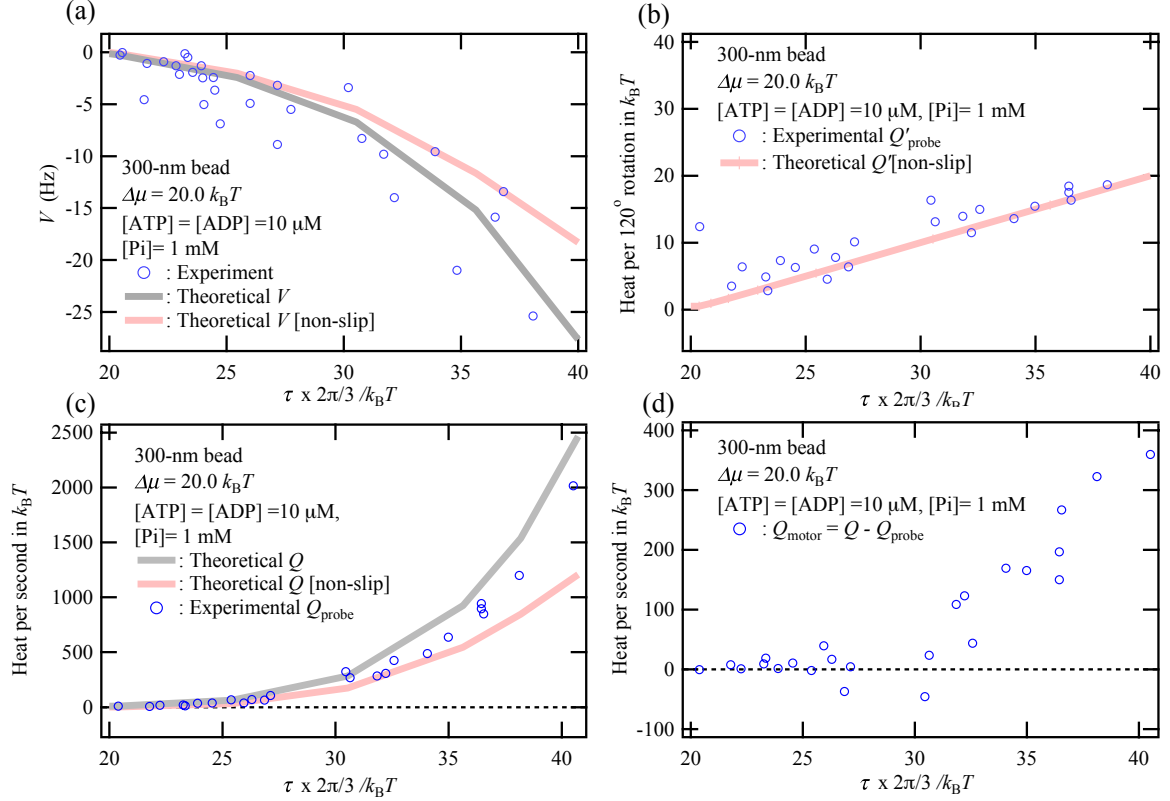
Figure 4. Mechanochemical coupling properties of the F₁ synthase. (a) The rotation rates V determined by the experiment [64], the eight-state model, and the non-slip model; (b) heat per 120° clockwise rotation given by the non-slip model, Q'[non-slip], and experimentally determined heat that irreversibly dissipates through the viscous friction of the probe, Q'_{probe} [64]; (c) heat per unit time given by the experimental data using $Q_{probe} = 3|V| \times Q'_{probe}$, that by the eight-state model, Q, and that by the non-slip model, Q[non-slip]; (d) heat per unit time, that directly dissipates from the F₁ synthase calculated on the basis of both the experimental results and the theoretical results by the eight-state model, $Q_{motor} = Q - Q_{probe}$, are shown as a function of external torque $(\tau \times 2\pi/3)/k_BT$ under the condition of $\Delta\mu = 20.0 k_BT$ where [ATP]=[ADP]=10 μM and [Pi]=1 mM. In (c), Q and Q[non-slip] are given by $-2\pi\tau V - \Delta\mu\Delta J$[synthesis], while the experimental Q_{probe} is determined via $Q_{probe} = 3|V| \times Q'_{probe}$ using V provided by the eight-state model shown (a). The experimental results shown here were provided by Toyabe *et al.* and used a 300-nm bead as the probe [64].

Phosphate release as the driving force of 40° substep. In this study, we have used a chemomechamical network approach to address the efficiency of chemomechanical free energy transduction in one of the paradigmatic molecular motors, the rotary motor F₁-ATPase. In addition to insight into the efficiency of the motor, our approach also sheds light on the kinetics of the motor as

12

represented by a network structure consisting of multiple mechanochemical cycles. Specifically, two models with the same network topology, but different chemical identities of the states, have been presented (Figs. 1b and 1d). In both models, ATP binding to the empty catalytic site at the loose packing state (the 3-to-1 transition) should be regarded as the trigger of the 80° substep, and subsequently the 80° rotation leads to the conformation transformation into the tight packing state. On the other hand, the impact of Pi release upon the 40° substep is different in the two models. In the model shown by Fig. 1b, Pi release (the 8-to-7 transition), resulting in an empty catalytic site, induces a large conformation change that can act as the trigger of the 40° substep. By contrast, in the model shown in Fig. 1d, a large conformational change, sufficient to trigger the 40° substep, might not be explained by the Pi release, since ADP remains in the catalytic site.

Anyways, the obtained results with respect to the main working cycle and state probabilities at a saturating ATP concentration indicate that the 40° substep and Pi release are the first and second rate-limiting process, respectively, and the Pi release plays a crucial role on the torque generation by the 40° substep (see Fig. S6a). These results are consistent with experimentally observed high probability of 80° dwell [18] (see Fig. 1c). The primary rate-limiting 40° substep is triggered by the second rate-limiting Pi release following the 40° rotation. The γ-subunit-angle dependence of Pi affinity experimentally observed by Watanabe et al. [62] suggests a large conformation change due to the Pi release. The second rate-limiting slow Pi release, which is also consistent with molecular dynamics simulations [44-46], would be responsible for the large conformation change that triggers the 40° substep. All these theoretical, computational, and experimental observations support the reaction scheme given by Fig. 1b rather than by Fig. 1d.

$\Delta\mu$-dependent efficiencies of F$_1$-ATPase. F$_1$-ATPase is a reversible rotary motor that also works as an ATP synthase under forced reverse rotation, which is also its function in vivo, where the rotation is driven by the F$_o$ subunit of the F$_o$-F$_1$ ATP synthase. In contrast to the two-headed linear molecular motors, kinesin-1 and myosin V, this reversibility suggests a high free-energy transduction efficiency of F$_1$-ATPase. On the basis of precise single-molecule experimental data by Toyabe et al. [10] a possibility of nearly 100% free-energy transduction efficiency by F$_1$-ATPase has been suggested. Here we have analyzed this issue with a chemomechanical network approach. Our quantitative analysis indicates that mechanical slip that occurs under high external torque needs to be incorporated into the model to explain the experimental data. The occurrence of mechanical slip limits the maximal efficiency to ~80% [see Fig. 3c] as a result of a trade-off between a reduction in the heat that dissipates through the viscous friction of the probe and an increase in the heat caused by the mechanical slip with increasing external torque. How can the free-energy transduction and ATP synthesis efficiencies by F$_1$-ATPase be increased to be closer to the perfect free-energy transduction?

Our results show that the maximal work W_{stall} approaches the value of the non-slip model as the chemical potential difference $\Delta\mu$ decreases (Figs. S3a and S3b). This is because the stall torque τ_{stall} depends on $\Delta\mu$, such that the higher $\Delta\mu$ the larger the stall torque τ_{stall}. As a consequence, the free-energy transduction efficiency η_{m} approaches the perfect efficiency as $\Delta\mu$ decreases, whereas the maximum of work done by the motor, i.e., W_{stall} decreases. In the same manner, the ATP synthesis efficiency by forced reverse rotation of F_1-ATPase is affected by $\Delta\mu$ (Figs. S5a and S5b). Under physiological conditions, the synthesis efficiency is much higher than under the experimental conditions considered here (compare Fig. S5a and S5b) due to a lower $\Delta\mu$. In vivo, a high Pi concentration decreases $\Delta\mu$ and boosts the efficiency of ATP synthesis.

Concluding remarks. We presented a chemomechanical network model of F_1-ATPase that provides a quantitative description of the rotary motor dynamics driven by ATP hydrolysis as well as ATP synthesis caused by forced reverse rotation. The network model exhibits high reversibility, such that the ATP synthesis cycle corresponds to the reversal of ATP-driven motor cycle. However, our quantitative analysis demonstrated that torque-induced mechanical slip without any chemomechanical coupling occurs under high external torque. As a result, the free energy transduction efficiency is found to be rather high, but remains substantially below 100%. Thus, an important feature of F_1-ATPase is that the stall condition is not a thermodynamic equilibrium and heat is irreversibly dissipated due to mechanical slipping, so that F_1 consumes ATP in a futile manner, indicating that the optimal efficiency $\eta_{\text{m}} = 1$, cannot be achieved by F_1 even under stall torque conditions. Such irreversible heat dissipation at stall is a commonly observed phenomenon in biological nanomachines, since biomolecules are easily distorted by external force so that mechanical slips occur. In such imperfect chemomechanical coupling motors, the maximum transduction efficiency is governed by a trade-off between a reduction in heat dissipation through the viscous load and an increase in heat caused by the mechanical slip with increasing external force.

ASSOCIATED CONTENT

Supporting Information

The Supporting Information is available free of charge on the ACS Publications website at DOI: ……

Details of our model and calculation, an appendix, and additional results, as well as tables of model parameters are contained.

AUTHOR INFORMATION

Corresponding Author

*E-mail: sumi@okayama-u.ac.jp

ORCID

Tomonari Sumi: 0000-0002-4230-5908

Stefan Klumpp: 0000-0003-0584-2146

Notes

The authors declare no competing financial interest.

REFERENCES

(1)   Alberts, B.; Bray, D.; Hopkin, K.; Johnson, A. D.; Lewis, J.; Raff, M.; Roberts, K.; Walter, P. *Essential Cell Biology, 4th edition*; Garland Science: New York, 2013.

(2)   Lipowsky, R.; Klumpp, S. *Physica A: Statistical Mechanics and its Applications* **2005**, *352* (1), 53–112.

(3)   Seifert, U. *The European Physical Journal B* **2008**, *64* (3), 423–431.

(4)   Jarzynski, C. *Annual Review of Condensed Matter Physics* **2011**, *2*, 329–351.

(5)   Seifert, U. *Rep Prog Phys* **2012**, *75* (12), 126001.

(6)   Noji, H.; Yasuda, R.; Yoshida, M.; Kinosita, K. *Nature* **1997**, *386* (6622), 299–302.

(7)   Schnitzer, M. J.; Visscher, K.; Block, S. M. *Nat Cell Biol* **2000**, *2* (10), 718–723.

(8)   Schief, W. R.; Clark, R. H.; Crevenna, A. H.; Howard, J. *Proc. Natl. Acad. Sci. U.S.A.* **2004**, *101* (5), 1183–1188.

(9)   Toyabe, S.; Okamoto, T.; Watanabe-Nakayama, T.; Taketani, H.; Kudo, S.; Muneyuki, E. *Phys. Rev. Lett.* **2010**, *104* (19).

(10)   Toyabe, S.; Watanabe-Nakayama, T.; Okamoto, T.; Kudo, S.; Muneyuki, E. *PNAS* **2011**, *108* (44), 17951–17956.

(11)   BOYER, P. D. *Biochim Biophys Acta* **1993**, *1140* (3), 215–250.

(12)   Senior, A. E.; Nadanaciva, S.; Weber, J. *Biochimica et Biophysica Acta (BBA) - Bioenergetics* **2002**, *1553* (3), 188–211.

(13)   Kinosita, K.; Adachi, K.; Itoh, H. *Annu Rev Biophys Biomol Struct* **2004**, *33*, 245–268.

(14)   Junge, W.; Sielaff, H.; Engelbrecht, S. *Nature* **2009**, *459* (7245), 364–370.

(15)   Abrahams, J. P.; Leslie, A. G.; Lutter, R.; Walker, J. E. *Nature* **1994**, *370* (6491), 621–628.

(16)   Kinosita, K.; Yasuda, R.; Noji, H.; Adachi, K. *Philos. Trans. R. Soc. Lond., B, Biol. Sci.* **2000**,

355 (1396), 473–489.

(17)   Weber, J.; Senior, A. E. *Biochim Biophys Acta* **2000**, *1458* (2-3), 300–309.

(18)   Yasuda, R.; Noji, H.; Yoshida, M.; Kinosita, K.; Itoh, H. *Nature* **2001**, *410* (6831), 898–904.

(19)   Itoh, H.; Takahashi, A.; Adachi, K.; Noji, H.; Yasuda, R.; Yoshida, M.; Kinosita, K. *Nature* **2004**, *427* (6973), 465–468.

(20)   Rondelez, Y.; Tresset, G.; Nakashima, T.; Kato-Yamada, Y.; Fujita, H.; Takeuchi, S.; Noji, H. *Nature* **2005**, *433* (7027), 773–777.

(21)   Carter, N. J.; Cross, R. A. *Nature* **2005**, *435* (7040), 308–312.

(22)   Liepelt, S.; Lipowsky, R. *J Stat Phys* **2010**, *141* (1), 1–16.

(23)   Sumi, T. *Sci. Rep.* **2017**, *7* (1), 1163.

(24)   Gebhardt, J. C. M.; Clemen, A. E. M.; Jaud, J.; Rief, M. *Proc. Natl. Acad. Sci. U.S.A.* **2006**, *103* (23), 8680–8685.

(25)   Sumi, T. *Sci. Rep.* **2017**, *7* (1), 13489.

(26)   Hyeon, C.; Klumpp, S.; Onuchic, J. N. *Phys Chem Chem Phys* **2009**, *11* (24), 4899–4910.

(27)   Zimmermann, E.; Seifert, U. *New J. Phys.* **2012**, *14* (10), 103023.

(28)   Nishiyama, M.; Higuchi, H.; Yanagida, T. *Nat Cell Biol* **2002**, *4* (10), 790–797.

(29)   Kolomeisky, A. B. *Motor Proteins and Molecular Motors*, 1st ed.; CRC Press, 2015.

(30)   Ariga, T.; Tomishige, M.; Mizuno, D. *Phys. Rev. Lett.* **2018**, *121* (21), 218101.

(31)   Hendricks, A. G. *Physics* **2018**, *11*, 120–122.

(32)   Hwang, W.; Hyeon, C. *J. Phys. Chem. Lett.* **2018**, *9* (3), 513–520.

(33)   Yasuda, R.; Noji, H.; Kinosita, K.; Yoshida, M. *Cell* **1998**, *93* (7), 1117–1124.

(34)   Muneyuki, E.; Watanabenakayama, T.; Suzuki, T.; Yoshida, M.; Nishizaka, T.; Noji, H. *Biophysical Journal* **2007**, *92* (5), 1806–1812.

(35)   Toyabe, S.; Ueno, H.; Muneyuki, E. *Europhysics Letters* **2012**, *97* (4), 40004–.

(36)   Toyabe, S.; Muneyuki, E. *Biophysics (Nagoya-shi)* **2013**, *9*, 91–98.

(37)   Böckmann, R. A.; Grubmüller, H. *Nat Struct Biol* **2002**, *9* (3), 198–202.

(38)   Koga, N.; Takada, S. *Proc. Natl. Acad. Sci. U.S.A.* **2006**, *103* (14), 5367–5372.

(39)   Pu, J.; Karplus, M. *PNAS* **2008**, *105* (4), 1192–1197.

(40)   Ito, Y.; Ikeguchi, M. *J. Comput. Chem.* **2010**, *31* (11), 2175–2185.

(41)   Ito, Y.; Oroguchi, T.; Ikeguchi, M. *J. Am. Chem. Soc.* **2011**, *133* (10), 3372–3380.

(42)   Yoshidome, T.; Ito, Y.; Ikeguchi, M.; Kinoshita, M. *J. Am. Chem. Soc.* **2011**, *133* (11), 4030–4039.

(43)   Czub, J.; Grubmüller, H. *PNAS* **2011**, *108* (18), 7408–7413.

(44)   Ito, Y.; Yoshidome, T.; Matubayasi, N.; Kinoshita, M.; Ikeguchi, M. *J Phys Chem B* **2013**, *117* (12), 3298–3307.

(45)   Okazaki, K.-I.; Hummer, G. *PNAS* **2013**, *110* (41), 16468–16473.

(46)   Ito, Y.; Ikeguchi, M. *Biophysical Journal* **2015**, *108* (1), 85–97.

(47)   Okazaki, K.-I.; Hummer, G. *Proc. Natl. Acad. Sci. U.S.A.* **2015**, *112* (34), 10720–10725.

(48)   Wang, H. Y.; Oster, G. *Nature* **1998**, *396* (6708), 279–282.

(49)   Sun, S.; Wang, H.; Oster, G. *Biophysical Journal* **2004**, *86* (3), 1373–1384.

(50)   Gaspard, P.; Gerritsma, E. *Journal of theoretical biology* **2007**, *247* (4), 672–686.

(51)   Gerritsma, E.; Gaspard, P. *Biophysical Reviews and Letters* **2010**, *05* (04), 163–208.

(52)   Kawaguchi, K.; Sasa, S.-I.; Sagawa, T. *Biophysical Journal* **2014**, *106* (11), 2450–2457.

(53)   Shinagawa, R.; Sasaki, K. *J. Phys. Soc. Jpn.* **2016**, *85* (6), 064004.

(54)   Li, C.-B.; Ueno, H.; Watanabe, R.; Noji, H.; Komatsuzaki, T. *Nat Commun* **2015**, *6* (1), 10223.

(55)   Liepelt, S.; Lipowsky, R. *Phys. Rev. Lett.* **2007**, *98* (2), 258102.

(56)   Lipowsky, R.; Liepelt, S. *J Stat Phys* **2008**, *130* (1), 39–67.

(57)   Lipowsky, R.; Liepelt, S.; Valleriani, A. *J Stat Phys* **2009**, *135* (5-6), 951–975.

(58)   Bierbaum, V.; Lipowsky, R. *Biophysical Journal* **2010**, *100* (7), 1747–1755.

(59)   Nishizaka, T.; Oiwa, K.; Noji, H.; Kimura, S.; Muneyuki, E.; Yoshida, M.; Kinosita, K. *Nat Struct Mol Biol* **2004**, *11* (2), 142–148.

(60)   Adachi, K.; Oiwa, K.; Nishizaka, T.; Furuike, S.; Noji, H.; Itoh, H.; Yoshida, M.; Kinosita, K. *Cell* **2006**, *130* (2), 309–321.

(61)   Watanabe, R.; Iino, R.; Noji, H. *Nat Chem Biol* **2010**, *6* (11), 814–820.

(62)   Watanabe, R.; Okuno, D.; Sakakihara, S.; Shimabukuro, K.; Iino, R.; Yoshida, M.; Noji, H. *Nat Chem Biol* **2011**, *8* (1), 86–92.

(63)   Adachi, K.; Oiwa, K.; Yoshida, M.; Nishizaka, T.; Kinosita, K. *Nat Commun* **2011**, *3*, 1022–1022.

(64)   Toyabe, S.; Muneyuki, E. *New J. Phys.* **2015**, *17* (1), 015008.

(65)   Elston, T.; Wang, H. Y.; Oster, G. *Nature* **1998**, *391* (6666), 510–513.

(66)   Dimroth, P.; Wang, H. Y.; Grabe, M.; Oster, G. *Proc. Natl. Acad. Sci. U.S.A.* **1999**, *96* (9), 4924–4929.

(67)   Oster, G.; Wang, H. Y. *J. Bioenerg. Biomembr.* **2000**, *32* (5), 459–469.

(68)   Adachi, K.; Yasuda, R.; Noji, H.; Itoh, H.; Harada, Y.; Yoshida, M.; Kinosita, K. *Proc. Natl. Acad. Sci. U.S.A.* **2000**, *97* (13), 7243–7247.

(69)   Shimabukuro, K.; Muneyuki, E.; Yoshida, M. *Biophys. J.* **2006**, *90* (3), 1028–1032.

(70)   Hirono-Hara, Y.; Noji, H.; Nishiura, M.; Muneyuki, E.; Hara, K. Y.; Yasuda, R.; Kinosita, K.; Yoshida, M. *Proc. Natl. Acad. Sci. U.S.A.* **2001**, *98* (24), 13649–13654.

(71)   Yoshidome, T.; Ito, Y.; Matubayasi, N.; Ikeguchi, M.; Kinoshita, M. *J Chem Phys* **2012**, *137*
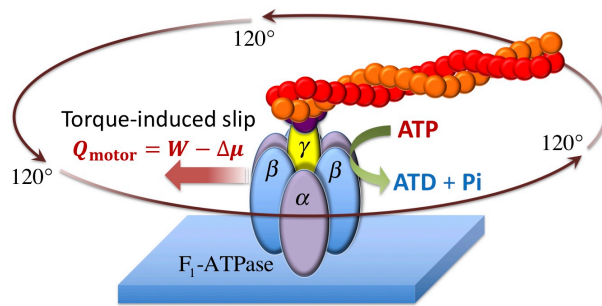
(3), 035102–035109.

(72)   Liepelt, S.; Lipowsky, R. *Europhys. Lett.* **2007**, *77* (5), 50002.

(73)   Hill, T. L. *Free energy transduction and biochemical cycle kinetics*; Springer: New York, 1989.

(74)   Palanisami, A.; Okamoto, T. *Nano Lett.* **2010**, *10* (10), 4146–4149.

(75)   Martin, J. L.; Ishmukhametov, R.; Spetzler, D.; Hornung, T.; Frasch, W. D. *PNAS* **2018**, *115* (22), 5750–5755.

TOC